SCIENTIFIC REPORTS

OPEN

Organic carbon budget for the eastern boundary of the North Atlantic subtropical gyre: major role of DOC in mesopelagic respiration

Yeray Santana-Falcón[1], Xosé Antón Álvarez-Salgado[2], María Dolores Pérez-Hernández[1,3], Alonso Hernández-Guerra[1], Evan Mason[4] & Javier Arístegui[1]

Transports of suspended particulate (POC_{susp}) and dissolved (DOC) organic carbon are inferred from a box-model covering the eastern boundary of the North Atlantic subtropical gyre. Corresponding net respiration rates (R) are obtained from a net organic carbon budget that is based on the transport estimates, and includes both vertical and lateral fluxes. The overall R in the mesopelagic layer (100–1500 m) is 1.6 ± 0.4 mmol C m^{-2} d^{-1}. DOC accounts for up to 53% of R as a result of drawdown of organic carbon within Eastern North Atlantic Central Water (ENACW) that is entrained into sinking Mediterranean Overflow Water (MOW) that leads to formation of Mediterranean water (MW) at intermediate depths (~900 m). DOC represents 90% of the respired non-sinking organic carbon. When converted into oxygen units, the computed net respiration rate represents less than half the oxygen utilization rates (OUR) reported for the mesopelagic waters of the subtropical North Atlantic. Mesoscale processes in the area, not quantified with our approach, could account in part for the OUR differences observed between our carbon budget and other published studies from the North Atlantic, although seasonal or interannual variability could also be responsible for the difference in the estimates.

Oceanic respiration occurs over the entire water column[1, 2], as opposed to photosynthesis, which is restricted to the epipelagic layer (roughly above 150 m). The non-respired fraction of the biogenic organic carbon produced in the epipelagic layer is susceptible to downward export in the form of dissolved (DOC) and particulate (POC) organic carbon, supporting respiration in the dark ocean[2, 3]. At the global scale, the relative contribution of DOC to oxygen consumption in the dark ocean has been estimated to be 10–20%[4, 5], but it may increase significantly in regions of deep-water convection[5–7]. Paradoxically, the sum of DOC and sinking POC collected with sediment traps does not frequently account for the estimated dark ocean respiration rates[8–10]. This conflicting imbalance could be a consequence of methodological uncertainties in the estimation of respiration rates and/or carbon fluxes[10–12]. For instance, the bulk of particulate material in the water column is composed of slow-settling or suspended particles[13–15] that can escape from sediment traps due to their buoyancy[16]. Several studies have suggested that suspended particles are an important source of organic matter for prokaryotic organisms in the mesopelagic zone[17, 18]. Therefore, suspended particles would represent an unquantified source of "missing" organic carbon, especially in areas where lateral advection is intense, such as in Eastern Boundary Current systems[19]. Indeed, it has been already shown that, using a box-model approach, suspended particulate organic carbon (POC_{susp}) could support up to 59% of the total mesopelagic respiration in the southwestern sector of the Canary Current[20], a region strongly affected by the coastal-ocean export of particulate material from the NW African coastal upwelling system[21, 22].

[1]Instituto de Oceanografía y Cambio Global, IOCAG, Universidad de Las Palmas de Gran Canaria, ULPGC, 35017, Las Palmas de Gran Canaria, Spain. [2]CSIC, Instituto de Investigaciones Marinas, Eduardo Cabello, 6, 36208, Vigo, Spain. [3]Department of Physical Oceanography, Woods Hole Oceanographic Institution, Woods Hole, Massachusetts, USA. [4]Instituto Mediterráneo de Estudios Avanzados, CSIC-UIB. C. Miquel Marquès, 21, 07190, Esporles, Illes Balears, Spain. Correspondence and requests for materials should be addressed to Y.S.-F. (email: yeray.santana@ulpgc.es)
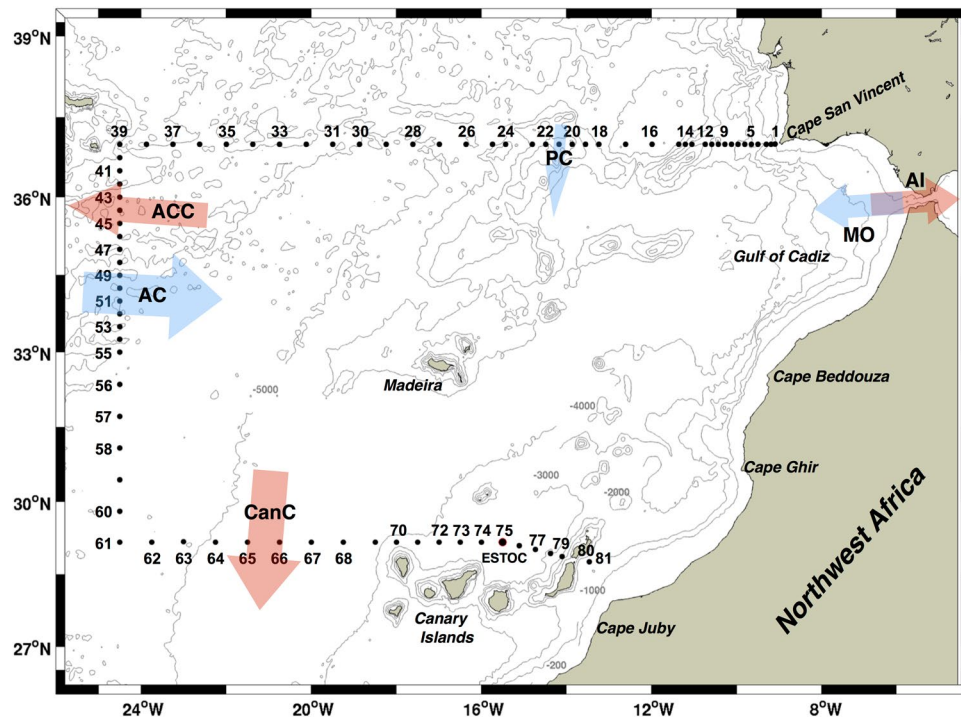
Figure 1. Location of the CTD stations. Biogeochemical stations are numbered. AC, ACC, CanC, and PC refer to Azores Current, Azores Counter-Current, Canary Current, and Portugal Current. AI and MO indicate the surface Atlantic inflow and bottom Mediterranean overflow. Blue/red arrows indicate transport into/out of the study region. Station 75 is at the ESTOC site. The map was produced using M_Map toolbox (https://www.eoas.ubc.ca/~rich/map.html) on MATLAB R2013a, https://www.mathworks.com/products/matlab/. Global ETOPO is used for bathymetric data (https://www.ngdc.noaa.gov/mgg/global/).

In the present study, following the approach used by Alonso-González and coworkers in the southern Canary Current[20], we estimate the contribution of DOC and POC_{susp} fluxes to net respiration in the eastern boundary of the North Atlantic subtropical gyre (Fig. 1). Our overarching hypothesis is that, contrary to the southern Canary Current where POC_{susp} is an important component of the carbon budget[20, 23], the DOC contribution to total respiration in the study area is larger than that of POC_{susp}. The two areas are oceanographically distinct. On the one hand, the coastline orientation in our region is unfavorable to coastal upwelling, which is absent or limited just to the summer months[24, 25]. On the other hand, our region is characterized by the density-driven exchange of water masses between the Mediterranean Sea and the eastern North Atlantic[26]. As a consequence, Eastern North Atlantic Central Water (ENACW) is entrained into the dense fast-flowing Mediterranean Overflow Water (MOW) that exits through the Strait of Gibraltar[27–29] and is subducted along the slope into the Gulf of Cádiz (ca. 33–37°N)[30–33] to below 1000 m depth, where it spreads into the Atlantic as Mediterranean Water (MW)[27–29, 34–37]. This entrainment of ENACW into MOW may promote the downward flux of DOC to intermediate layers in this particular region, as has already been shown for anthropogenic carbon dioxide[38].

In a previous study[39], based on a rough estimation of organic carbon fluxes in a box region that included the Strait of Gibraltar, it has been suggested that DOC remineralization could explain about 90% of the inorganic carbon produced in the water column. Our study tests this hypothesis, providing direct measurements of POC_{susp} and DOC fluxes for integration within a box-model analysis. We aim to contribute to the understanding of the organic carbon dynamics in this complex region, which is characterized by the confluence of water masses of different origin, water mass entrainment and subduction, and intermittent upwelling[24, 40–43].

Results

Organic carbon distributions. The DOC and POC_{susp} data used in this work were collected during a research cruise in autumn 2009. The cruise consisted of a set of hydrographic stations distributed regularly along three transects (northern, western and southern) that delimit the box presented in Fig. 1 (see Materials and Methods for further details on sampling and analysis). POC_{susp} and DOC distributions from 0 to 4000 m (Fig. 2) show that surface POC_{susp} concentrations along the northern transect decrease offshore from 4–6 µmol C L^{-1} in the coastal area to about 2 µmol C L^{-1} in the open ocean. Below 500 m POC_{susp} concentrations are 1 µmol C L^{-1} or less, except around a seamount at ~14° W. Waters with relatively high POC_{susp} deepen at station 30. Surface DOC concentrations are higher than 60 µmol C L^{-1} for the entire transect. A deepening of DOC occurs at stations 30–37.

Surface POC_{susp} concentrations along the western transect are higher than 1–2 µmol C L^{-1}. A deepening of POC_{susp}-rich waters at stations 56–58 coincides with the shoaling of isoneutral surfaces between two mesoscale
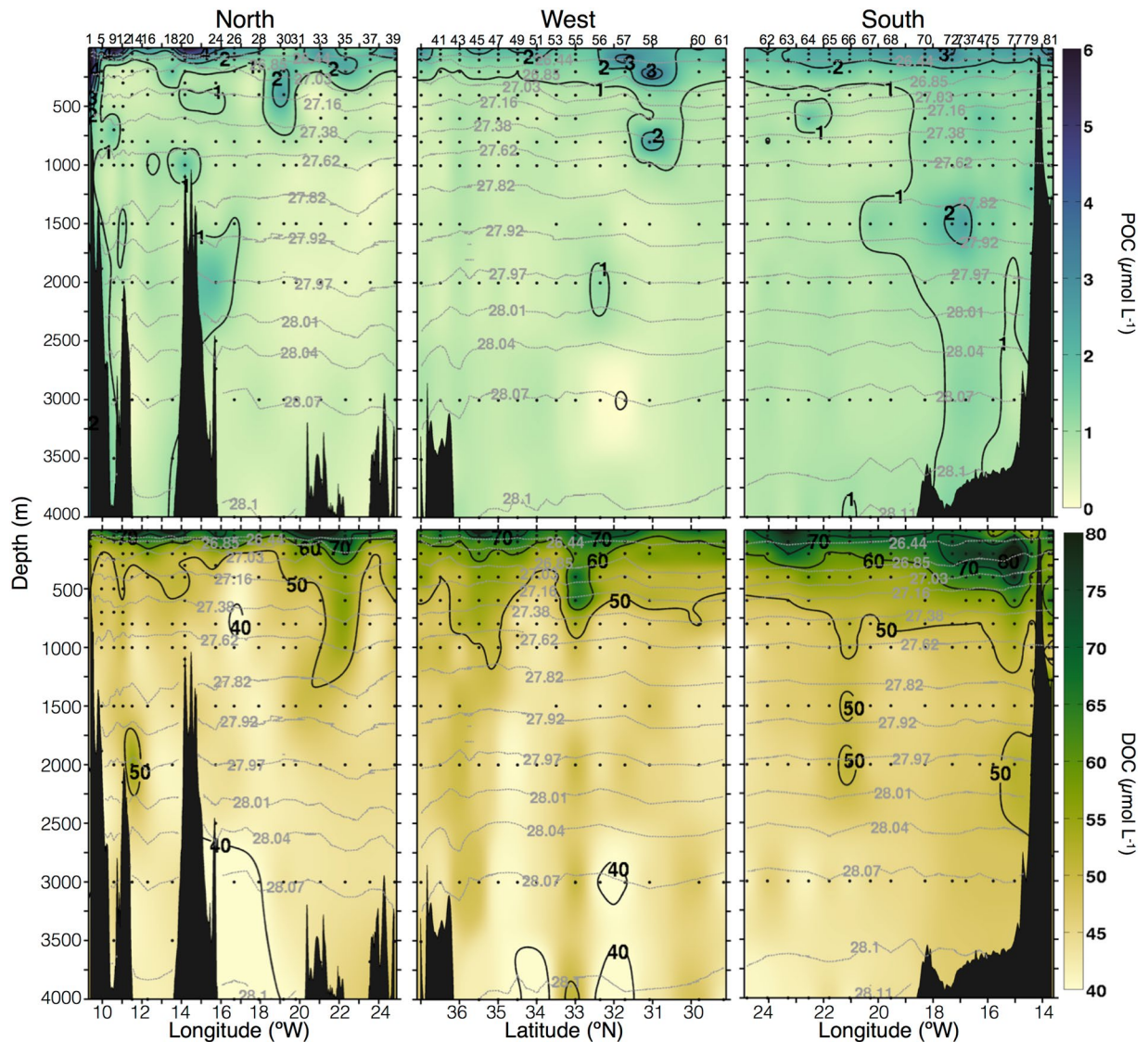
Figure 2. Vertical section (0–4000 m) of POC_{susp} (µmol C L^{-1}; upper panels) and DOC (µmol C L^{-1}; lower panels) for the northern (left), western (middle), and southern (right) transects. Biogeochemical stations are indicated at the top of the upper panels. Gray dotted lines indicate neutral density.

eddies[44]. POC_{susp} concentrations remain around 1 µmol C L^{-1} along the rest of the section with little variation. DOC is about 60–70 µmol C L^{-1} near the surface, and decreases to less than 50 µmol C L^{-1} with depth. Central waters with high DOC concentrations descend along sloping isoneutrals at stations 53–56. The deepening of DOC north of 35°N coincides with the location of the Azores Current system[44].

The southern transect shows surface POC_{susp} concentrations of 2–3 µmol C L^{-1}. A westward decrease is observed below 250 m. Surface DOC concentrations show values above 70–80 µmol C L^{-1}. A patch of relatively high POC_{susp} below 1000 m depth coincides with cool and fresh waters[44]. DOC shows values above 70–80 µmol C L^{-1} at the surface, with maximum concentrations above 100 µmol C L^{-1} at subsurface depths (~200 m) in the eastern stations close to the Lanzarote Passage. Intermediate waters (below the 27.38 isoneutral) show low DOC concentrations, except at stations 64–65 where a front between a cyclonic eddy and the southward Canary Current is periodically observed[44].

Mass transports.   Mass transports across the northern, western, and southern transects are taken from a previous study by Pérez-Hernandez and co-workers who developed an inverse box model with data from the same cruise[44] (see Material and Methods for further details about the inverse model and its reliability). A summary of the integrated lateral mass transport at each transect is presented in Fig. 3. Note that fluxes into/out of the box are indicated by positive/negative signs, respectively.

A predominant inward (southward) transport is observed across the northern transect (~37°N; blue line), interrupted only by the outward (northward) transport of intermediate waters (isoneutrals 27.38 to 27.92). The mass transport across the western transect (~24°W; red line) is strongly inwards (eastward) in the surface and
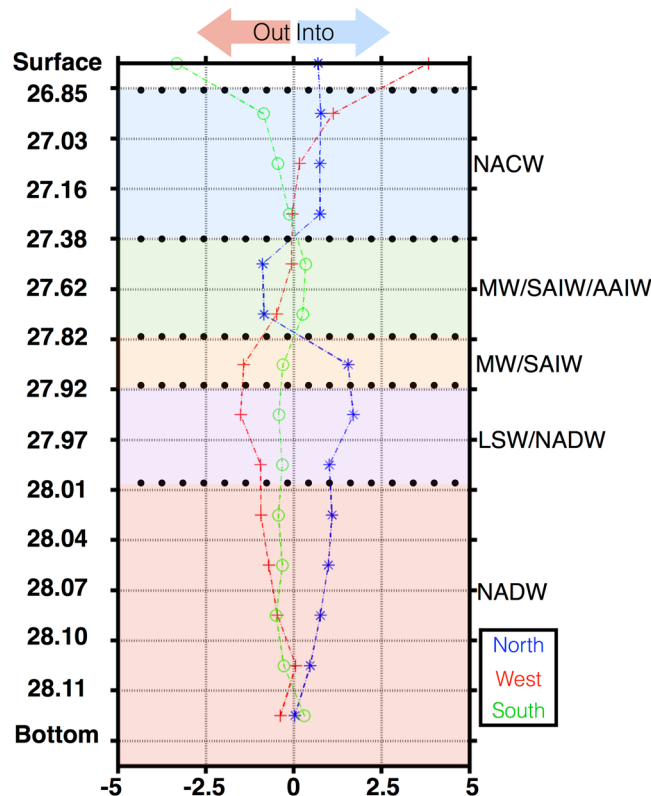
Figure 3. Integrated mass transports for the northern (blue diamonds over a dashed line), western (red crosses over a dotted line) and southern (green circle dashed line) transects. The sign of the net transport is negative/positive for diverging/converging flow out of/into the box. North Atlantic Central Water (NACW), Mediterranean Water (MW), sub-Artic Intermediate Water (SAIW), Antarctic Intermediate Water (AAIW), Labrador Sea Water (LSW), and North Atlantic Deep Water (NADW) water masses are indicated both by color and acronym. Y-axis is neutral density.

central waters, and predominantly outwards (westward) below. The mass transport across the southern transect (~29°N; green line) is outwards (southward) in the upper 700 meters of the water column, while the flow of intermediate and deep waters varies by less than ±2 Sv.

POC$_{susp}$ and DOC transports. Organic carbon transports along isoneutrals are calculated by multiplying the corresponding POC$_{susp}$ and DOC concentrations (Fig. 2) by the mass transports (Fig. 3) (see Materials and Methods for more details on the estimation and robustness of the carbon transports). For the case of DOC, transports of the non-refractory pool DOC (e-DOC) are calculated. The e-DOC pool is obtained by subtracting a background refractory DOC concentration (~45 mmol C m^{-3} in the study area) from the measured DOC. We only consider the e-DOC fraction because the refractory fraction renewal is thousands of years[45, 46], a period much longer than the decadal renewal time for the study box.

POC$_{susp}$ and e-DOC transports in the area (Fig. 4) may be divided into a southward flux of surface and central waters, interrupted by a weak northward transport of the upper intermediate waters, that is observed both at the northern and southern transects. Southward transport prevails again in the deepest waters. The zonal circulation is predominantly eastward at the surface and central waters. The trend reverses in the intermediate and deep layers where a westward transport is observed, especially at the bottom of the intermediate layer.

POC$_{susp}$ and e-DOC fluxes in the surface, central, intermediate, and deep waters at each transect are summarised in Table 1. The inputs (positive values) of organic carbon through the northern and western transects exceed the outputs (negative values) of the southern transect at both surface and central layers. Weak horizontal output fluxes are found both in the intermediate and the deepest layers.

Discussion

To evaluate the organic carbon sources within the box we build a mass balance (Fig. 5a) and an associated organic carbon budget (Fig. 5b). For the surface waters (0–100 m), 1.2 ± 0.1 Sv enter the box through the northern, southern and western transects, and −0.78 ± 0.1 Sv leave the box as the Atlantic inflow into the Mediterranean Sea (see Materials and Methods). As a result, the mass balance of inputs minus outputs to the box would be 0.4 ± 0.2 Sv. We propose that this volume is transported from the surface to the central waters to partially balance the loss of ENACW to intermediate waters when entrained into the MOW (see below the discussion about the mass balance of the central waters). The balance of organic carbon, i.e. POC$_{susp}$ and e-DOC, transported across the northern, western and southern transects indicates that the surface waters of the box receive an external input from the
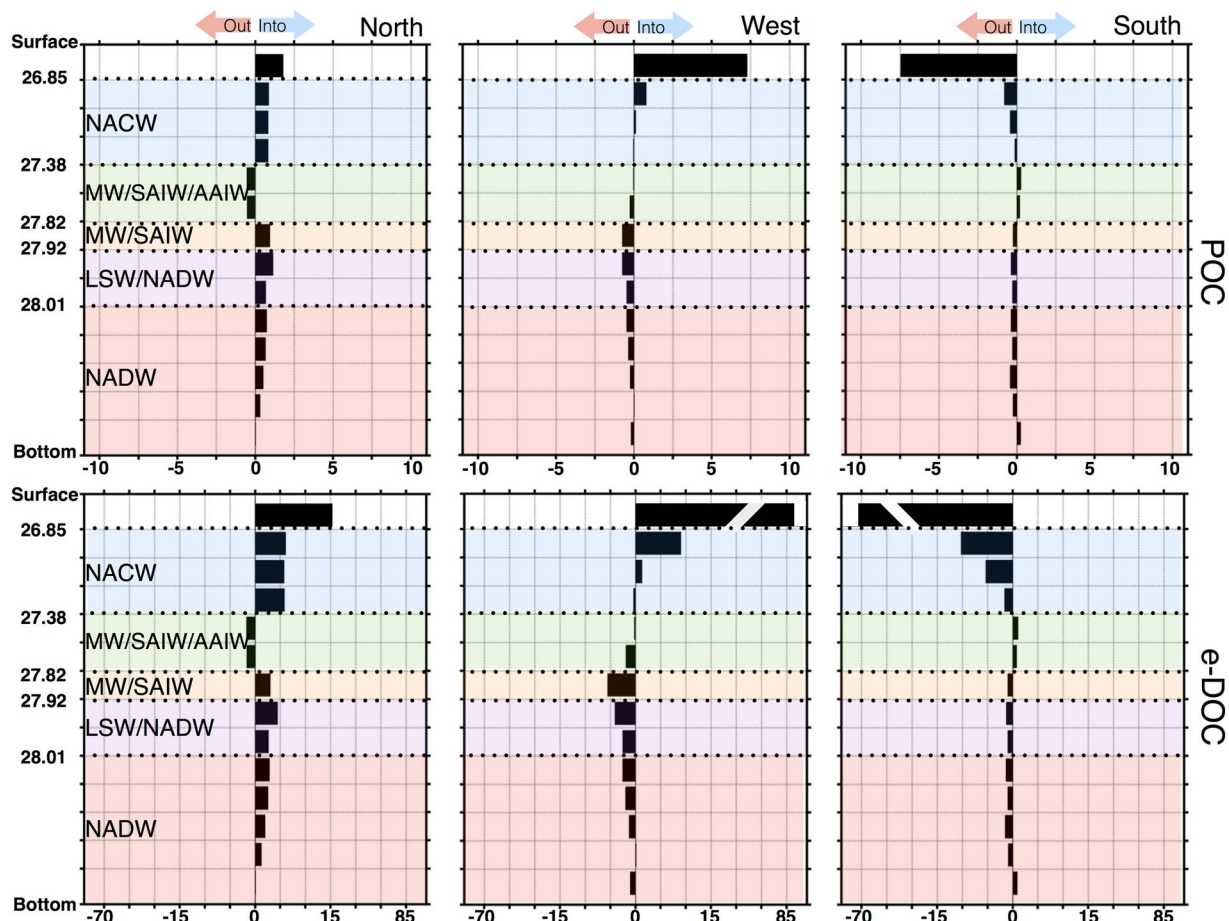
Figure 4. POC$_{susp}$ (upper panels) and DOC (lower panels) fluxes (10^8 mol C d^{-1}) at each transect. Positive/negative values indicate inputs/outputs to/from the box. Water masses are indicated both by color and acronym: North Atlantic Central Water (NACW), Mediterranean Water (MW), sub-Arctic Intermediate Water (SAIW), Antarctic Intermediate Water (AAIW), Labrador Sea Water (LSW), and North Atlantic Deep Water (NADW). Y-axes is neutral density.

	Northern Transect		Western Transect		Southern Transect		Global	
	POC$_{susp}$	e-DOC	POC$_{susp}$	e-DOC	POC$_{susp}$	e-DOC	POC$_{susp}$	e-DOC
Surface	1.79 ± 0.02	15.29 ± 0.04	7.27 ± 0.2	85.20 ± 2.8	−7.45 ± 0.5	−70.46 ± 3.1	**1.48 ± 0.2**	**28.51 ± 2.0**
Central	2.52 ± 0.3	17.83 ± 2.3	0.87 ± 0.03	9.97 ± 0.7	−1.34 ± 0.1	−17.46 ± 2.9	**1.93 ± 0.2**	**−0.12 ± 0.06**
Intermediate	−0.12 ± 0.06	−0.39 ± 0.2	−1.03 ± 0.09	−7.73 ± 0.9	0.22 ± 0.01	0.88 ± 0.02	**−0.96 ± 0.1**	**−7.53 ± 0.5**
Deep	4.04 ± 0.4	16.04 ± 1.5	−2.41 ± 0.3	−13.24 ± 0.9	−1.68 ± 0.1	−5.95 ± 0.5	**−0.24 ± 0.3**	**−3.79 ± 1.0**

Table 1. POC$_{susp}$ and e-DOC fluxes (10^8 mol C d^{-1}) for surface, central, intermediate, and deep waters for the northern, western, and southern transects. Error bars are given. Positive/negative values indicate input/outputs to/from the box.

Atlantic Ocean of $30.0 \pm 2.0 \times 10^8$ mol C d^{-1}. At the same time, according to our estimates (see Materials and Methods), $-11.4 \pm 2.9 \times 10^8$ mol C d^{-1} is exported within surface waters to the Mediterranean Sea. This number lies within the range of the Atlantic inflow of TOC previously measured in April 1998 (7.6×10^8 mol C d^{-1})[47], and in September 1997 (27.1×10^8 mol C d^{-1})[48], after subtraction of refractory DOC.

Furthermore, the non-respired organic carbon in surface waters may be transported to the dark ocean by turbulent diffusion, passive sinking, and active transport[49, 50]. We estimated first the vertical turbulent diffusion at 100 m depth as $F = -\varepsilon \times R/(N^2 \times (1 - R)) \times (DOC_{z2} - DOC_{z1})/(z_2 - z_1)$[51]. We considered (1) the averaged DOC in the upper 100 m (DOC_{z1} centered at $z_1 = 50$ m) and from 100 to 200 m depth (DOC_{z2}, centered at $z_2 = 150$ m) for the calculation of the vertical DOC gradient, (2) the square of the Brunt-Väisälä frequency (N^2) between 50 and 150 m, and (3) constant values for the dissipation rate ($\varepsilon = 10^{-8}$ m^3 s^{-2}) and the Richardson number ($R = 0.2$). We obtained an averaged value of 0.4 ± 0.3 mmol C m^{-2} d^{-1}, (average ± SD of 47 stns) that would give a total downward DOC flux of about $5.7 \pm 3.7 \times 10^8$ mol C d^{-1}, when multiplied by the surface area of the box (1.4×10^6 km^2).
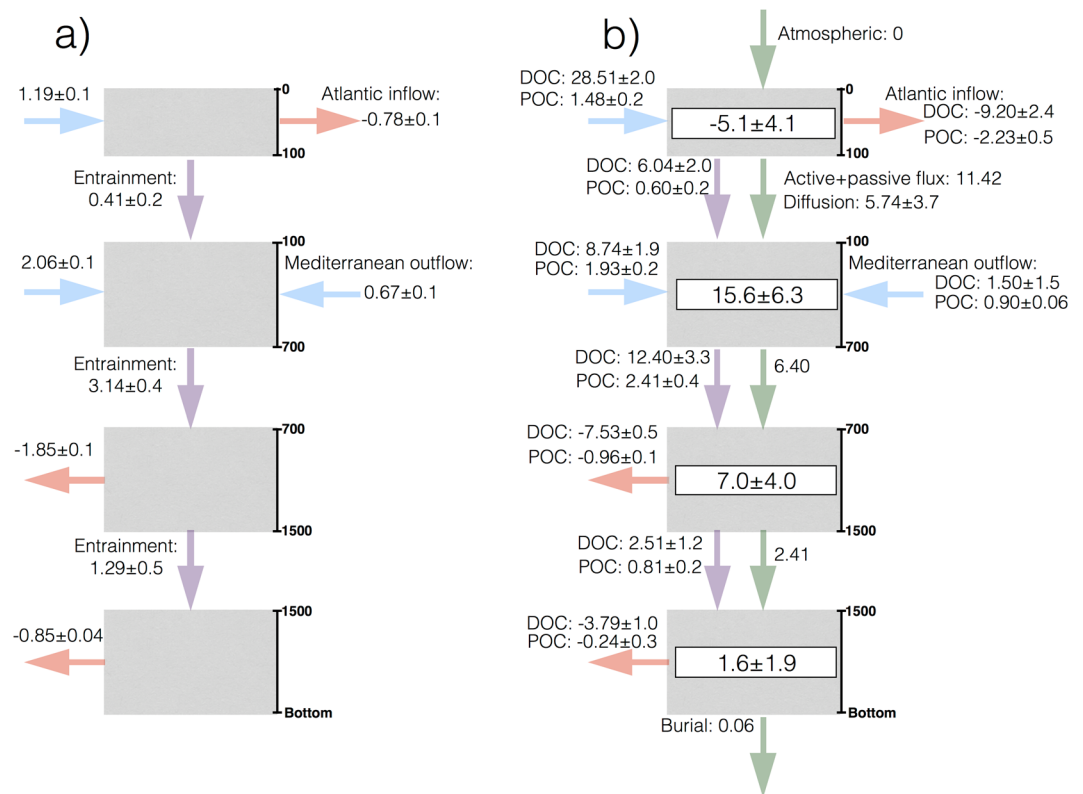
Figure 5. Schematic diagram showing (**a**) the mass transport and (**b**) the organic carbon budgets in the box region. The water column is divided into surface (0–100 m), central (100–700 m), intermediate (700–1500 m), and deep (below 1500 m) layers. Arrows indicate net transport (Sv) or organic carbon (10^8 mol C d^{-1}) across the open boundaries. Light blue indicates lateral inputs (positive values), light red indicates lateral outputs (negative values), light violet indicates vertical entrainment, light green indicates vertical fluxes from the layer above. Net respiration rates for each compartment are indicated.

Sinking POC fluxes obtained with surface tethered traps at 200 m depth and extrapolated to 150 m with the Martin equation[52] were approximately 0.55 mmol C m^{-2} d^{-1} at the European Station for Time-series in the Ocean (ESTOC)[53]. In the northeast Atlantic (39–43°N, 17–19°W), the minimum vertical POC fluxes were estimated to be 0.36 ± 0.09 mmol C m^{-2} d^{-1} from drifting traps at 200 m depth during late summer[54]. Although the use of drifting traps has been frequently criticized for underestimating export fluxes[55–57], comparison with POC fluxes at the Bermuda Time Series Station (BATS) derived from both surface-tethered traps and Thorium-234[56] shows reasonable agreement during low productivity periods. At the ESTOC site, the lowest productivity values have been obtained during autumn (~10 mmol C m^{-2} d^{-1})[57]; considering an e-ratio (export/production ratio) of 5–10%[55], the vertical POC flux during the less productive season would be 0.5–1.0 mmol C m^{-2} d^{-1}. Therefore, an average value of the export rate from drifting traps of 0.36 to 1.0 mmol C m^{-2} d^{-1} is representative of the sinking flux from surface waters within the box at that time of the year. Aggregation and disaggregation of sinking particles by biotic and abiotic mechanisms could modify the sinking rates and magnitude of POC fluxes with depth across the dark ocean[58–62], although our box model approach does not allow identification of these processes.

In addition, the estimated averaged vertical flux of POC mediated by migrant zooplankton (active flux) was 0.22 mmol C m^{-2} d^{-1} south of the island of Gran Canaria[63], accounting for 25% of the sinking POC flux (passive flux) in the region. More recently, a mean active flux of 0.28 mmol C m^{-2} d^{-1} (29% of the passive flux) has been estimated north of Gran Canaria[64]; these estimates agree with those observed at BATS (0.17 mmol C m^{-2} d^{-1})[65] and the Hawaiian Ocean Time Series (HOT; 0.26 mmol C m^{-2} d^{-1})[66]. However, the active flux accounted for only 8% and 11–44% of the passive flux at their respective regions[65, 66]. If we assume that the active flux represents at best 20% of the passive flux in our region, the passive + migratory POC flux from the surface to the central waters would be around 0.82 mmol C m^{-2} d^{-1} which, multiplied by the area of our box, yields a total POC flux from the surface to the central waters of 11.4×10^8 mol C d^{-1}.

The central waters (100–700 m) within the box receive an overall lateral input of POC$_{susp}$ and e-DOC of $10.7 \pm 1.9 \times 10^8$ mol C d^{-1} from the surrounding Atlantic Ocean and $2.4 \pm 1.5 \times 10^8$ mol C d^{-1} from the Mediterranean outflow through the Strait of Gibraltar. In addition, it is well known that MOW is subducted within the study box to more than 1000 m and that the central waters are entrained into the MOW as it sinks[29, 38]. In fact, the mass balance of central waters within the box (Fig. 5a), considering the net water flows across the northern, southern, and western transects (2.1 ± 0.1 Sv), the Mediterranean outflow into the Atlantic (0.67 ± 0.1 Sv; see Materials and Methods), and the input of 0.4 ± 0.2 Sv from the surface waters, is 3.1 ± 0.4 Sv. Therefore, in order to maintain conservation of volume in the central waters, 3.1 ± 0.4 Sv should enter the intermediate layer by

entrainment of the central waters into the subducting Mediterranean outflow. Our volume calculation is in agreement with earlier estimates (2–3 Sv[67]; 2.6 Sv[68]; 1.3 Sv[28]; 2.3 Sv[38]). To obtain the organic carbon transported by this volume, we multiply the average organic carbon concentration at the bottom of the central layer by 3.1 ± 0.4 Sv to obtain a downward POC + e-DOC flux of $14.8 \pm 3.7 \times 10^8$ mol C d^{-1}, 90% of which is DOC. Similarly, we also calculate the organic carbon transport associated with the 0.4 ± 0.2 Sv of surface waters that enter the central waters yielding $6.6 \pm 2.2 \times 10^8$ mol C d^{-1}, 10% as POC$_{susp}$ and 90% as DOC (Fig. 5b).

For the intermediate waters (700–1500 m), aside from the organic carbon that enters this layer by entrainment of ENACW into the subducting MOW ($14.8 \pm 3.7 \times 10^8$ mol C d^{-1}), the other organic carbon transports associated with the water mass fluxes leave this layer. The net balance of POC$_{susp}$ and e-DOC transport across the northern, western and southern transects is $-8.5 \pm 0.6 \times 10^8$ mol C d^{-1}. This indicates an export from the box to the adjacent Atlantic Ocean, and is especially intense across the western transect (see Table 1), contrary to the surface and central waters where organic carbon was imported from the Atlantic Ocean. Furthermore, the mass balance of the intermediate waters (Fig. 5a) indicates that there should be an entrainment of 1.3 ± 0.5 Sv into the deep waters for volume conservation, that translates into a drawdown of organic carbon of $3.3 \pm 1.4 \times 10^8$ mol C d^{-1}, 76% of which is DOC (Fig. 5b). In addition, an average particle flux below 700 m of 0.46 mmol C m^{-2} d^{-1} has been obtained from three sites located within the Canary Current region[69]. Assuming this value for our region of study, we obtain a vertical POC supply to intermediate waters of 6.4×10^8 mol C d^{-1}.

Finally, the mass transport balance of the deep waters (below 1500 m), 0.4 ± 0.4 Sv, is compatible with mass conservation within the uncertainty of the estimates. POC$_{susp}$ + e-DOC transported from the intermediate waters by entrainment ($3.3 \pm 1.4 \times 10^8$ mol C d^{-1}), sinking POC (2.4×10^8 mol C d^{-1}), organic carbon burial into the sediments (0.06×10^8 mol C d^{-1})[70], and the carbon balance at the open boundaries of the box ($-4.0 \pm 1.3 \times 10^8$ mol C d^{-1}) yield a negligible carbon excess of $1.6 \pm 1.9 \times 10^8$ mol C d^{-1}. The sinking POC flux at 1500 m was derived from the flux at 700 m using the Martin equation[52].

Overall, the organic carbon balance for the surface waters associated with the lateral fluxes across the northern, western and southern transects ($30.0 \pm 2.2 \times 10^8$ mol C d^{-1}), losses from the Strait of Gibraltar ($-11.4 \pm 2.9 \times 10^8$ mol C d^{-1}), entrainment ($-6.6 \pm 2.0 \times 10^8$ mol C d^{-1}), active + passive transport fluxes (-11.4×10^8 mol C d^{-1}), and turbulent diffusion ($-5.7 \pm 3.7 \times 10^8$ mol C d^{-1}), yields $-5.1 \pm 4.1 \times 10^8$ mol C d^{-1}. Assuming steady state conditions, this balance results in a net heterotrophy (R > 0) of about -0.4 ± 0.3 mmol C m^{-2} d^{-1} at the time of this study.

The overall balance of organic carbon for the central waters includes the POC$_{susp}$ + DOC lateral fluxes across the Atlantic boundaries of the box ($10.7 \pm 2.1 \times 10^8$ mol C d^{-1}; 82% as DOC) and the Strait of Gibraltar ($2.4 \pm 1.6 \times 10^8$ mol C d^{-1}; 62% DOC), passive + active fluxes of POC from surface waters (11.4×10^8 mol C d^{-1}), and to intermediate waters (-6.4×10^8 mol C d^{-1}), downward DOC fluxes by turbulent diffusion ($5.7 \pm 3.7 \times 10^8$ mol C d^{-1}), and entrainment from the surface ($6.6 \pm 2.2 \times 10^8$ mol C d^{-1}), and to the intermediate waters ($-14.8 \pm 3.7 \times 10^8$ mol C d^{-1}). All these organic carbon fluxes result in a net R of $15.6 \pm 6.3 \times 10^8$ mol C d^{-1} (1.1 ± 0.4 mmol C m^{-2} d^{-1}).

Lastly, for intermediate waters the POC$_{susp}$ + e-DOC includes the balance across the northern, western and southern boundaries ($-8.5 \pm 0.6 \times 10^8$ mol C d^{-1}), entrainment from central waters ($14.8 \pm 3.7 \times 10^8$ mol C d^{-1}) and into deeper waters ($-3.3 \pm 1.4 \times 10^8$ mol C d^{-1}), and vertical downward POC fluxes from central waters (6.40×10^8 mol C d^{-1}) and to deeper layers (-2.4×10^8 mol C d^{-1}), resulting in a net R of $7.0 \pm 4.0 \times 10^8$ mol C d^{-1} (0.5 ± 0.3 mmol C m^{-2} d^{-1}) assuming steady-state conditions.

The net R within the mesopelagic layer, assumed to be equivalent to the sum of the central and the intermediate waters, is $22.7 \pm 5.2 \times 10^8$ mol C d^{-1} (1.6 ± 0.4 mmol C m^{-2} d^{-1}). This value is lower than those obtained with a similar box model west of the Canary Islands[20]: 2.4–5.1 mmol C m^{-2} d^{-1}. According to these authors, POC$_{susp}$ would support 28–59% of the total mesopelagic R in that region. However, their estimates were based solely on POC$_{susp}$ fluxes, assuming two scenarios in which the contribution of DOC was fixed at 15 and 30%. In the present study, we have measured DOC and calculated that it contributes about 53% to total mesopelagic R within the box. It has been hypothesized that DOC represents about 90% of the respiration of non-sinking organic carbon in the mesopelagic layer from an empirical carbon mass balance within a box bounded by the Strait of Gibraltar, 24–41° N and 22° W[39]. Our results indicate that DOC represents that fraction when only the non-sinking organic carbon is considered, in agreement with the high DOC consumption rates obtained in areas undergoing water mass transformation[6, 71].

The estimated mesopelagic R is much lower than the oxygen utilization rates (OUR) calculated for the North Atlantic subtropical gyre[72–74] (9–11 mmol C m^{-2} d^{-1} as converted using a -O$_2$/C molar ratio of 1.4[75]). In addition, a carbon budget north of our box region during summer 2009[76] estimated a total input of organic carbon to the twilight zone (ca. 50–1000 m) of ~7.7 mmol C m^{-2} d^{-1}, due mainly to sinking POC. OUR values ranging from 4.7 to 16.6 mmol C m^{-2} d^{-1} between 100 to 750 m depth were obtained using tritium and ^{228}Ra methodologies in the North Atlantic subtropical gyre[77]. Similar integrated values (4.9 to 13.0 mmol C m^{-2} d^{-1}) of carbon respiration for the 100–1000 depth zone were obtained both by ^{7}Be and POC flux attenuation methodologies in the subtropical North Atlantic[78]. A compilation of data from the Pacific ocean[79] shows OUR values ranging from 0.04 to 18.1 mmol C m^{-2} d^{-1}. In the North Pacific, OUR values integrated over the first 600 m depth[80] averaged 4.6 mmol C m^{-2} d^{-1}, while higher OUR values of 9.8 to 11.7 mmol C m^{-2} d^{-1} have been recently reported for a monthly time-series at HOT[12]. Values obtained during the present study might, however, underestimate the annual mean since our study took place during the unproductive autumn when POC$_{susp}$ concentrations are particularly low[56]. Additionally, the region within the box is strongly influenced by mesoscale features such as filaments and eddies, whose effects on carbon sequestration remain to be quantified. The enhancement of carbon fluxes to the ocean interior driven by mesoscale eddies has been reported in a number of studies[81–88]. Indeed, injection of organic carbon from surface waters was especially intense in several areas, such as in the anticyclonic eddy at the northwestern corner of the box (stations 33–35), or the Azores Front (stations 52–55[44]). Moreover,

upwelling filaments may play a key role in the coastal-ocean transport of organic matter[89, 90]. The Cape Ghir filament lies within the region of study, and may export to the open ocean 29 to 63% of the annual averaged primary production associated with the coastal upwelling[91, 92]. All of these features occur episodically within the box, and could enhance the supply of organic carbon to mesopelagic waters.

Near the ESTOC site, net R rates at the mesopelagic zone (ca. 150–700 m) of 2.0–3.1 mol C m^{-2} y^{-1} (5.5–8.5 mmol C m^{-2} d^{-1}) were obtained by using a tracer conservation model applied to climatological data[93]. They also obtain consistent R rates based on ETS (electron transport system) respiratory activity for the same region at the end of March. Differences between these estimates and our values could be due to higher lateral advection of DOC and POC$_{susp}$ from the coastal upwelling region at that site[56], and higher productivity at the end of the late winter bloom.

In summary, this study provides an estimate of net respiration in the mesopelagic waters within a box enclosing the eastern boundary of the North Atlantic subtropical gyre. This estimate is based on the assumption that the box is in steady state, i.e., there is neither accumulation of organic carbon entering the box nor consumption of previously accumulated organic carbon. This assumption is acceptable for the budget of the central, intermediate, and deep waters as their decadal renewal times preclude seasonality. However, seasonal variability is pronounced in the surface layer and, hence, the steady state assumption could lead to biased values of the annual net fluxes. Furthermore, although the contribution of mesoscale phenomena needs to be addressed in future studies, our results show that a major fraction of the mesopelagic organic carbon demand in this area is fuelled by DOC. Indeed, the formation of MW has been found to be the main mechanism for the export of anthropogenic carbon in this region[38]. Despite the inaccuracy of the steady-state assumption the carbon budget presented here shows that the vertical entrainment of ENACW into subducting MOW contributes to the export of DOC to mesopelagic waters, where it may constitute the main substrate supporting dark ocean respiration. Likewise, due to the westward advection of intermediate waters, this process may also represent a significant supply of organic carbon to the eastern North Atlantic outside the box.

Materials and Methods

Hydrography and seawater sampling. Between October 15 and November 11, 2009 the RV *Hespérides* carried out an intensive hydrographic survey in the eastern boundary of the North Atlantic subtropical gyre at the confluence region between the Azores Current System, the Portugal Current and the Canary Current. A grid of 81 conductivity-temperature-depth (CTD) stations was distributed along a box region defined by 28.7–37.0°N and 24.5°W. At 47 of these stations seawater samples were taken for analysis of dissolved (DOC) and particulate organic carbon (POC; Fig. 1, numbered dots).

Readers interested in a detailed description of the hydrography and water mass characterization are referred to Pérez-Hernández and coworkers[44].

Organic carbon. Discrete samples of POC were obtained at selected depths from the surface up to the bottom (5, 25, 50, 100 200, 400, 600, 800, 1000, 1500, 2000, 3000, 4000 and 5000 m) by means of a rosette sampler equipped with twenty-four 10 L Niskin bottles. Although we are aware that particles sink at different rates, we assume that all the POC collected in oceanographic bottles corresponds to the slowly-settling or suspended pool (POC$_{susp}$)[20]. Thus, this pool represents an upper threshold for the particulate organic material that is susceptible to lateral transport. Water samples (4 L) for POC$_{susp}$ were collected in polypropylene bottles and filtered through precombusted (450 °C, 12 hours) 25 mm Whatman GF/F-filters (pore size 0.7 µm). The filters were wrapped in precombusted aluminium foil and frozen at −20 °C. In the laboratory, the filters were thawed and dried overnight at 55 °C, then placed overnight in a desiccator saturated with HCl fumes to remove inorganic carbon, and dried again in a second desiccator with silica gel for at least 24 hours. Finally, the filters were packed in tin sleeves before being analysed with a Perkin-Elmer 2400 CHN elemental analyser following standard protocols[94]. Unused pre-combusted GF/F-filters were treated in the same way and used as handling blanks. Blanks ranged from 0.06 to 0.7 µmol C L^{-1}. DOC adsorption onto the filters was estimated at several random stations, at three different depth levels, as the amount of carbon retained on a backing filter placed underneath the main filter. The values ranged from 0.17 to 1.73 µmol C per 25 mm-diameter GF/F-filter, which are similar to previous estimates[20, 95, 96].

At the same stations and depth levels, samples for the analyses of DOC were collected in 250 mL acid-cleaned all-glass flasks. Samples from the upper 100 m were immediately filtered through precombusted (450 °C, 4 hours) 47 mm Whatman GF/F filters in an acid-cleaned all-glass filtration system. Filtered surface and unfiltered deeper water samples were collected in 10 mL precombusted glass ampules (450 °C, 12 hours). After acidification with H$_3$PO$_4$, the ampoules were heat-sealed and preserved in the dark at 4 °C until analysis in the laboratory with a Shimadzu TOC-V organic carbon analyser by high temperature catalytic oxidation (HTCO). The system was calibrated daily with potassium hydrogen phthalate (99.95–100.05%, p.a., Merck). The precision of the DOC calibration was ± 1 µmol L^{-1}. The performance of the instrument was tested with the carbon reference materials (CRM) provided by D. A. Hansell (University of Miami, USA). Measured concentrations of the CRM were 45.5 ± 1.7 µmol C (n = 10); the certified value is 44–46 µmol C L^{-1} (lot#09-06 from the Florida Strait at 700 m).

Organic carbon budget. The water column was divided into discrete neutral density layers[97]. The upper four layers coincide roughly with the main thermocline waters (below 27.38 neutral density layers; 0–700 m), the following three layers with intermediate waters (27.38–27.92; 700–1500 m), and the lowest seven layers with deep waters (27.92–28.10; below 1500 m). Our estimates were based on the inverse box model used by Pérez-Hernández and coworkers[44] to obtain mass transports (M) for each layer along the northern, western, and southern transects. The model uses the thermal wind equation after calculating the reference level velocities and their uncertainties. These velocities are calculated assuming geostrophy, and mass and property conservation. The inverse box model used has been extended from a previous one[98] to include the approximate conservation of mass

and anomalies of salinity and heat, and to allow transfer between layers. This model also considers adjustment of fresh water fluxes and Ekman transports in each section. The inverse problem consists of 37 equations and 130 unknowns: 99 for reference velocities, 26 for vertical velocities and vertical diffusion, 4 for Ekman transports and 1 for the freshwater flux. To solve the inverse problem, the Gauss-Markov method, which produces a minimum error variance solution from initial estimates of the unknowns, was used. M at each layer is multiplied by the averaged suspended and dissolved organic carbon concentrations (C) at the same layer to obtain the corresponding lateral carbon fluxes (M × C). To report these carbon fluxes, the layers were grouped into surface, central, intermediate, and deep waters. The lateral carbon fluxes were summed to obtain the corresponding carbon budgets for each layer.

The robustness of the carbon fluxes and budgets calculated in this study was tested by means of the following perturbation test (see supplementary material): carbon fluxes were calculated as (M ± erM) × (C ± erC), where erM and erC represent the uncertainty of the estimation of M and C, respectively. Therefore, the values of M and C are perturbed within the limits of the uncertainty of their respective estimations. A total of 100 perturbations were performed for each carbon flux and budget. The average of these 100 values is considered the optimum solution and the corresponding standard deviation (SD) an estimate of the uncertainty of the fluxes and budgets[99]. See Pérez-Hernández and coworkers[44] for a thorough analysis of the values of M and erM used in the present calculations. Concerning the uncertainty of POC_{susp} and DOC measurements, these were obtained by calculating the SD of all suspended and dissolved organic carbon measured in each layer at each transect.

To obtain the organic carbon fluxes into/out of the Mediterranean Sea, mass transports across the Strait of Gibraltar were set at -0.78 ± 0.1 Sv for the surface outflow to the Mediterranean and 0.68 ± 0.1 Sv for the bottom inflow to the eastern North Atlantic[100] ($1\,Sv = 10^9\,kg\,s^{-1}$). These mass transports, which are within the range of other estimates in the literature[101–107], were multiplied by the average concentrations of POC_{susp} ($3.4\,mmol\,m^{-3}$ in the outflow and $1.6\,mmol\,m^{-3}$ in the inflow) and e-DOC ($13.7\,mmol\,m^{-3}$ in the outflow and $2.7\,mmol\,m^{-3}$ in the inflow) measured in the same region by Arístegui and co-workers (unpublished data from May 2014).

Net respiration (R) of POC_{susp} and e-DOC within each layer of the box is obtained as follows:

$$\frac{dTOC}{dt} = I - O - R \tag{1}$$

Assuming steady state conditions (dTOC/dt = 0), the balance of inputs (I) minus outputs (O) of total organic carbon ($TOC = POC_{susp} + e\text{-}DOC$) across the open boundaries must equal the total net respiration within the box;, i.e., R = I − O.

Data Availability.
The datasets generated during and/or analysed during the current study are available from the corresponding author on reasonable request.

References

1. Pomeroy, L. R. & Johannes, R. E. Occurrence and respiration of ultraplankton in the upper 500 meters of the ocean. *Deep Sea Research and Oceanographic Abstracts* **15**, 381–391 (1968).
2. del Giorgio, P. & Duarte, C. M. Respiration in the open ocean. *Nature* **420**, 379–384 (2002).
3. Arístegui, J. *et al.* Respiration in the dark ocean. *Geophys. Res. Lett.* **30** (2003).
4. Arístegui, J. *et al.* Dissolved organic carbon support of respiration in the dark ocean. *Science.* **298**, 1967 (2002).
5. Carlson, C. A. *et al.* Dissolved organic carbon export and subsequent remineralization in the mesopelagic and bathypelagic realms of the North Atlantic basin. *Deep Sea Res. Part II Top. Stud. Oceanogr.* **57**, 1433–1445 (2010).
6. Hansell, D. A., Carlson, C. A. & Suzuki, Y. Dissolved organic carbon export with North Pacific Intermediate Water formation. *Global Biogeochem. Cycles* **16** (2002).
7. Hansell, D., Carlson, C. A., Repeta, D. J. & Schlitzer, R. Dissolved Organic Matter in the Ocean. *Oceanography* **22**, 202–11 (2009).
8. Arístegui, J. *et al.* Respiration in the mesopelagic and bathypelagic zones of the oceans. *Respir. Aquat. Ecosyst.* **181** (2005).
9. Reinthaler, T. *et al.* Prokaryotic respiration and production in the meso-and bathypelagic realm of the eastern and western North Atlantic basin. *Limnol. & Oceanogr.* **51**, 1262–1273 (2006).
10. Burd, A. B. *et al.* Assessing the apparent imbalance between geochemical and biochemical indicators of meso- and bathypelagic biological activity: What the @$#! is wrong with present calculations of carbon budgets? *Deep. Res. Part II Top. Stud. Oceanogr.* **57**, 1557–1571 (2010).
11. Herndl, G. J. & Reinthaler, T. Microbial control of the dark end of the biological pump. *Nat. Geosci.* **6**, 718–724 (2013).
12. Martínez-García, S. Microbial respiration in the mesopelagic zone at Station ALOHA. *Limnol. & Oceanogr.* **62**, 320–333 (2017).
13. McCave, I. N. Size spectra and aggregation of suspended particles in the deep ocean. *Deep Sea Res. Part A. Oceanogr. Res. Pap.* **31**, 329–352 (1984).
14. Kepkay, P. E. Colloids and the ocean carbon cycle. in *Marine Chemistry* 35–56 (Springer, 2000).
15. Verdugo, P. *et al.* The oceanic gel phase: a bridge in the DOM–POM continuum. *Mar. Chem.* **92**, 67–85 (2004).
16. Trull, T. W. *et al.* In situ measurement of mesopelagic particle sinking rates and the control of carbon transfer to the ocean interior during the Vertical Flux in the Global Ocean (VERTIGO) voyages in the North Pacific. *Deep Sea Res. Part II Top. Stud. Oceanogr.* **55**, 1684–1695 (2008).
17. Karl, D. M., Knauer, G. A. & Martin, J. H. Downward flux of particulate organic matter in the ocean: a particle decomposition paradox. *Nature* **332**, 438–441 (1988).
18. Baltar, F. *et al.* Evidence of prokaryotic metabolism on suspended particulate organic matter in the dark waters of the subtropical North Atlantic. *Limnol. & Oceanogr.* **54**, 182–193 (2009).
19. Fischer, G., Reuter, C., Karakas, G., Nowald, N. & Wefer, G. Offshore advection of particles within the Cape Blanc filament, Mauritania: Results from observational and modelling studies. *Prog. Oceanogr.* **83**, 322–330 (2009).
20. Alonso-González, I. J. *et al.* Lateral POC transport and consumption in surface and deep waters of the Canary Current region: a box model study. *Global Biogeochem. Cycles* **23** (2009).
21. Pelegrí, J. L. *et al.* Nutrient irrigation of the North Atlantic. *Prog. Oceanogr.* **70**, 366–406 (2006).
22. Mason, E., Colas, F. & Pelegrí, J. L. A Lagrangian study tracing water parcel origins in the Canary Upwelling System. *Scientia Marina* **76** (2012).
23. Alonso-González, I. J. *et al.* Role of slowly settling particles in the ocean carbon cycle. *Geophys. Res. Lett.* **37** (2010).

24. Nykjaer, L. & Camp, L. Van. Seasonal and interannual variability of coastal upwelling along northwest Africa and Portugal from 1981 to 1991. *Journal of Geophysical Research* **99**, 197–207 (1994).

25. Benazzouz, A. *et al*. An improved coastal upwelling index from sea surface temperature using satellite-based approach –The case of the Canary Current upwelling system. *Cont. Shelf Res.* **81**, 38–54 (2014).

26. Bryden, H. L. & Stommel, H. M. Limiting processes that determine basic features of the circulation in the Mediterranean-Sea. *Oceanol. Acta* **7**, 289–296 (1984).

27. Price, J. F., Baringer, M. O., Lueck, R. G., Johnson, G. C. & Ambar, I. *Mediterranean outflow mixing dynamics* (1993).

28. Baringer, M. O. & Price, J. F. Mixing and Spreading of the Mediterranean Outflow. *J. Phys. Oceanogr.* **27**, 1654–1677 (1997).

29. Mauritzen, C., Morel, Y. & Paillet, J. On the influence of Mediterranean water on the central waters of the North Atlantic Ocean. *Deep Sea Res. Part I Oceanogr. Res. Pap.* **48**, 347–381 (2001).

30. Batteen, M. L., Martinez, J. R., Bryan, D. W. & Buch, E. J. A modeling study of the coastal eastern boundary current system off Iberia and Morocco. *J. Geophys. Res. Ocean.* **105**, 14173–14195 (2000).

31. García Lafuente, J. & Ruiz, J. The Gulf of Cádiz pelagic ecosystem: A review. *Prog. Oceanogr.* **74**, 228–251 (2007).

32. Peliz, A., Dubert, J., Marchesiello, P. & Teles-Machado, A. Surface circulation in the Gulf of Cadiz: Model and mean flow structure. *J. Geophys. Res. Ocean.* **112** (2007).

33. Peliz, A. *et al*. Surface circulation in the Gulf of Cadiz: 2. Inflow-outflow coupling and the Gulf of Cadiz slope current. *J. Geophys. Res. Ocean.* **114** (2009).

34. van Aken, H. M. The hydrography of the mid-latitude northeast Atlantic Ocean: I: The deep water masses. *Deep Sea Res. Part I Oceanogr. Res. Pap.* **47**, 757–788 (2000).

35. Fusco, G., Artale, V., Cotroneo, Y. & Sannino, G. Thermohaline variability of Mediterranean Water in the Gulf of Cadiz, 1948–1999. *Deep Sea Res. Part I Oceanogr. Res. Pap.* **55**, 1624–1638 (2008).

36. Carracedo-Segade, L. I., Gilcoto, M., Mercier, H. & Pérez, F. F. Quasi-synoptic transport, budgets and water mass transformation in the Azores-Gibraltar Strait region during summer 2009. *Prog. Oceanogr.* **130**, 47–64 (2015).

37. Carracedo-Segade, L. I., Pardo, P. C., Flecha, S. & Pérez, F. F. On the Mediterranean Water Composition. *J. Phys. Oceanogr.* **46**, 1339–1358 (2016).

38. Álvarez, M., Pérez, F. F., Shoosmith, D. R. & Bryden, H. L. Unaccounted role of Mediterranean Water in the drawdown of anthropogenic carbon. *J. Geophys. Res. Ocean.* **110** (2005).

39. Xose, S. *et al*. Biogeochemical budgets in the eastern boundary current system of the North Atlantic: Evidence of net heterotrophy and nitrogen fixation. *Limnol. & Oceanogr.* **52**, 1328–1335 (2007).

40. Benazzouz, A. *et al*. On the temporal memory of coastal upwelling off NW Africa. *J. Geophys. Res. Ocean.* **119**, 6356–6380 (2014).

41. Cropper, T. E., Hanna, E. & Bigg, G. R. Spatial and temporal seasonal trends in coastal upwelling off Northwest Africa, 1981–2012. *Deep Sea Res. Part I Oceanogr. Res. Pap.* **86**, 94–111 (2014).

42. Desbiolles, F. *et al*. Short-term upwelling events at the western African coast related to synoptic atmospheric structures as derived from satellite observations. *J. Geophys. Res. Ocean.* **119**, 1–23 (2014).

43. Desbiolles, F., Blanke, B., Bentamy, A. & Grima, N. Origin of fine-scale wind stress curl structures in the Benguela and Canary upwelling systems. *J. Geophys. Res. Ocean.* **119**, 7931–7948 (2014).

44. Pérez-Hernández, M. D. *et al*. The source of the Canary current in fall 2009. *J. Geophys. Res. Ocean.* **118**, 2874–2891 (2013).

45. Hansell, D. A. DOC in the global ocean carbon cycle. *Biogeochem. Mar. dissolved Org. matter* 685–715 (2002).

46. Hansell, D. A. Recalcitrant dissolved organic carbon fractions. *Ann. Rev. Mar. Sci.* **5**, 421–445 (2013).

47. Dafner, E. V., Sempéré, R. & Bryden, H. L. Total organic carbon distribution and budget through the Strait of Gibraltar in April 1998. *Mar. Chem.* **73**, 233–252 (2001).

48. Dafner, E., González-Dávila, M., Santana-Casiano, J. M. & Sempéré, R. Total organic and inorganic carbon exchange through the Strait of Gibraltar in September 1997. *Deep Sea Res. Part I Oceanogr. Res. Pap.* **48**, 1217–1235 (2001).

49. Ducklow, H. W., Steinberg, D. K. & Buesseler, K. O. Upper ocean carbon export and the biological pump. *Oceanography* **14**, 50–58 (2001).

50. Sanders, R. *et al*. The biological carbon pump in the North Atlantic. *Prog. Oceanogr.* **129**, 200–218 (2014).

51. Doval, M. D., Álvarez-Salgado, X. A. & Pérez, F. F. Organic matter distributions in the eastern North Atlantic-Azores Front region. *J. Mar. Syst.* **30**, 33–49 (2001).

52. Martin, J. H., Knauer, G. A., Karl, D. M. & Broenkow, W. W. VERTEX: carbon cycling in the northeast Pacific. *Deep Sea Res. Part A. Oceanogr. Res. Pap.* **34**, 267–285 (1987).

53. Neuer, S., Freudenthal, T., Davenport, R., Llinás, O. & Rueda, M. J. Seasonality of surface water properties and particle flux along a productivity gradient of NW Africa. *Deep Sea Res. Part II Top. Stud. Oceanogr.* **49**, 3561–3576 (2002).

54. Goutx, M. *et al*. Particle flux in the northeast Atlantic Ocean during the POMME experiment (2001): Results from mass, carbon, nitrogen, and lipid biomarkers from the drifting sediment traps. *J. Geophys. Res. Ocean.* **110** (2005).

55. Buesseler, K. O. The decoupling of production and particulate export in the surface ocean. *Global Biogeochem. Cycles* **12**, 297–310 (1998).

56. Buesseler, K. O. *et al*. A comparison of the quantity and composition of material caught in a neutrally buoyant versus surface-tethered sediment trap. *Deep Sea Res. Part I Oceanogr. Res. Pap.* **47**, 277–294 (2000).

57. Neuer, S. *et al*. Biogeochemistry and hydrography in the eastern subtropical North Atlantic gyre. Results from the European time-series station ESTOC. *Prog. Oceanogr.* **72**, 1–29 (2007).

58. Bory, A. *et al*. Downward particle fluxes within different productivity regimes off the Mauritanian upwelling zone (EUMELI program). *Deep Sea Res. Part I Oceanogr. Res. Pap.* **48**, 2251–2282 (2001).

59. Kriest, I. & Evans, G. T. Representing phytoplankton aggregates in biogeochemical models. *Deep Sea Res. Part I Oceanogr. Res. Pap.* **46**, 1841–1859 (1999).

60. Kriest, I. Different parameterizations of marine snow in a 1D-model and their influence on representation of marine snow, nitrogen budget and sedimentation. *Deep Sea Res. Part I Oceanogr. Res. Pap.* **49**, 2133–2162 (2002).

61. Turner, J. T. Zooplankton fecal pellets, marine snow and sinking phytoplankton blooms. *Aquat. Microb. Ecol.* **27**, 57–102 (2002).

62. Karakaş, G. *et al*. High-resolution modeling of sediment erosion and particle transport across the northwest African shelf. *J. Geophys. Res.* **111** (2006).

63. Hernández-León, S. *et al*. Vertical distribution of zooplankton in Canary Island waters: implications for export flux. *Deep Sea Res. Part I Oceanogr. Res. Pap.* **48**, 1071–1092 (2001).

64. Ariza, A., Garijo, J. C., Landeira, J. M., Bordes, F. & Hernández-León, S. Migrant biomass and respiratory carbon flux by zooplankton and micronekton in the subtropical northeast Atlantic Ocean (Canary Islands). *Prog. Oceanogr.* **134**, 330–342 (2015).

65. Steinberg, D. K. *et al*. Zooplankton vertical migration and the active transport of dissolved organic and inorganic carbon in the Sargasso Sea. *Deep. Res.* **47**, 137–158 (2000).

66. Steinberg, D. K., Cope, J. S., Wilson, S. E. & Kobari, T. A comparison of mesopelagic mesozooplankton community structure in the subtropical and subarctic North Pacific Ocean. *Deep Sea Res. Part II Top. Stud. Oceanogr.* **55**, 1615–1635 (2008).

67. Zenk, W. On the Mediterranean outflow west of Gibraltar. *Meteor Forschungsergebnisse R. A, Allg. Phys. und Chemie des Meeres* **16**, 23–34 (1975).

68. Rhein, M. & Hinrichsen, H. H. Modification of Mediterranean Water in the Gulf of Cadiz, studied with hydrographic, nutrient and chlorofluoromethane data. *Deep Sea Res. Part I Oceanogr. Res. Pap.* **40**, 267–291 (1993).

69. Neuer, S. *et al.* Differences in the biological carbon pump at three subtropical ocean sites. *Geophys. Res. Lett.* **29** (2002).
70. Seiter, K., Hensen, C. & Zabel, M. Benthic carbon mineralization on a global scale. *Global Biogeochem. Cycles* **19** (2005).
71. Hansell, D. A. & Carlson, C. A. Deep-ocean gradients in the concentration of dissolved organic carbon. *Nature* **395**, 263–266 (1998).
72. Jenkins, W. J. & Goldman, J. C. Seasonal oxygen cycling and primary production in the Sargasso Sea. *J. Mar. Res.* **43**, 465–491 (1985).
73. Jenkins, W. J. Oxygen utilization rates in North Atlantic subtropical gyre and primary production in oligotrophic systems. *Nature* **300**, 246–248 (1982).
74. Jenkins, W. J. Studying subtropical thermocline ventilation and circulation using tritium and 3He. *J. Geophys. Res. Ocean.* **103**, 15817–15831 (1998).
75. Anderson, L. A. On the hydrogen and oxygen content of marine phytoplankton. *Deep sea Res. part I Oceanogr. Res. Pap.* **42**, 1675–1680 (1995).
76. Giering, S. L. C. *et al.* Reconciliation of the carbon budget in the ocean's twilight zone. *Nature* **507**, 480–483 (2014).
77. Sarmiento, J. L., Thiele, G., Key, R. M. & Moore, W. S. Oxygen and nitrate new production and remineralization in the North Atlantic subtropical gyre. *J. Geophys. Res. Ocean.* **95**, 18303–18315 (1990).
78. Kadko, D. Rapid oxygen utilization in the ocean twilight zone assessed with the cosmogenic isotope ^{7}Be. *Global Biogeochem. Cycles* **23** (2009).
79. Feely, R. A. *et al.* Oxygen utilization and organic carbon remineralization in the upper water column of the Pacific Ocean. *J. Oceanogr.* **60**, 45–52 (2004).
80. Sonnerup, R. E., Mecking, S. & Bullister, J. L. Transit time distributions and oxygen utilization rates in the Northeast Pacific Ocean from chlorofluorocarbons and sulfur hexafluoride. *Deep Sea Res. Part I Oceanogr. Res. Pap.* **72**, 61–71 (2013).
81. Bidigare, R. R. *et al.* Influence of a cyclonic eddy on microheterotroph biomass and carbon export in the lee of Hawaii. *Geophys. Res. Lett.* **30** (2003).
82. Sweeney, E. N., McGillicuddy, D. J. & Buesseler, K. O. Biogeochemical impacts due to mesoscale eddy activity in the Sargasso Sea as measured at the Bermuda Atlantic Time-series Study (BATS). *Deep Sea Res. Part II Top. Stud. Oceanogr.* **50**, 3017–3039 (2003).
83. McGillicuddy, D. J. *et al.* Eddy/wind interactions stimulate extraordinary mid-ocean plankton blooms. *Science* **316**, 1021–1026 (2007).
84. Alonso-González, I. J. *et al.* Regional and temporal variability of sinking organic matter in the subtropical northeast Atlantic Ocean: A biomarker diagnosis. *Biogeosciences* **7**, 2101–2115 (2010).
85. Alonso-González, I. J. *et al.* Carbon dynamics within cyclonic eddies: Insights from a biomarker study. *PLoS One* **8**, e82447 (2013).
86. Guidi, L. *et al.* Does eddy-eddy interaction control surface phytoplankton distribution and carbon export in the North Pacific Subtropical Gyre? *J. Geophys. Res.* **117** (2012).
87. Shih, Y.-Y. *et al.* Enhanced particulate organic carbon export at eddy edges in the oligotrophic western north pacific ocean. *PLoS One* **10**, e0131538 (2015).
88. Omand, M. M. *et al.* Eddy-driven subduction exports particulate organic carbon from the spring bloom. *Science* **348**, 222–225 (2015).
89. Gabric, A. J. *et al.* Offshore export of shelf production in the Cape Blanc (Mauritania) giant filament as derived from coastal zone color scanner imagery. *J. Geophys. Res.* **98**, 4697–4712 (1993).
90. Álvarez-Salgado, X. A. *et al.* Contribution of upwelling filaments to offshore carbon export in the subtropical Northeast Atlantic Ocean. *Limnol. & Oceanogr.* **52**, 1287–1292 (2007).
91. Garcia-Muñoz, M. *et al.* Exchange of carbon by an upwelling filament off Cape Ghir (NW Africa). *J. Mar. Syst.* **54**, 83–95 (2005).
92. Santana-Falcón, Y. *et al.* Coastal-offshore exchange of organic matter across the Cape Ghir filament (NW Africa) during moderate upwelling. *J. Mar. Syst.* **154**, 233–242 (2016).
93. Fernández-Castro, B. *et al.* Mesopelagic respiration near the ESTOC (European Station for Time-Series in the Ocean, 15.5° W, 29.1° N) site inferred from a tracer conservation model. *Deep Sea Res. Part I Oceanogr. Res. Pap.* **115**, 63–73 (2016).
94. UNESCO. Protocols for the Joint Global Ocean Flux Study (JGOFS) Core Measurement. *Intergov. Oceanogr. Comm. Man. Guid.* **29**, 169 (1994).
95. Moran, S. B., Charette, M. A., Pike, S. M. & Wicklund, C. A. Differences in seawater particulate organic carbon concentration in samples collected using small and large volume methods: the importance of DOC adsorption to the filter blank. *Mar. Chem.* **67**, 33–42 (1999).
96. Turnewitsch, R. *et al.* Determination of particulate organic carbon (POC) in seawater: The relative methodological importance of artificial gains and losses in two glass-fiber-filter-based techniques. *Mar. Chem.* **105**, 208–228 (2007).
97. Jackett, D. R. & McDougall, T. J. A Neutral Density Variable for the World's Oceans. *J. Phys. Oceanogr.* **27**, 237–263 (1997).
98. Joyce, T. M., Hernandez-Guerra, A. & Smethie, W. M. Zonal circulation in the NW Atlantic and Caribbean from a meridional World Ocean Circulation Experiment hydrographic section at 66° W. *J. Geophys. Res. Ocean.* **106**, 22095–22113 (2001).
99. Álvarez, M., Brea, S., Mercier, H. & Álvarez-Salgado, X. A. Mineralization of biogenic materials in the water masses of the South Atlantic Ocean. I: Assessment and results of an optimum multiparameter analysis. *Prog. Oceanogr.* **123**, 1–23 (2014).
100. Tsimplis, M. N. & Bryden, H. L. Estimation of the transports through the Strait of Gibraltar. *Deep Sea Res. Part I Oceanogr. Res. Pap.* **47**, 2219–2242 (2000).
101. Bryden, H. L., Candela, J. & Kinder, T. H. Exchange through the Strait of Gibraltar. *Prog. Oceanogr.* **33**, 201–248 (1994).
102. Baschek, B., Send, U., Lafuente, J. G. & Candela, J. Transport estimates in the Strait of Gibraltar with a tidal inverse model. *J. Geophys. Res.* **106**, 31–33 (2001).
103. García-Lafuente, J. *et al.* Low-frequency variability of the exchanged flows through the Strait of Gibraltar during CANIGO. *Deep Sea Res. Part II Top. Stud. Oceanogr.* **49**, 4051–4067 (2002).
104. García-Lafuente, J. *et al.* The very first transformation of the Mediterranean outflow in the Strait of Gibraltar. *J. Geophys. Res. Ocean.* **116** (2011).
105. Sánchez-Román, A., Sannino, G., García-Lafuente, J., Carillo, A. & Criado-Aldeanueva, F. Transport estimates at the western section of the Strait of Gibraltar: A combined experimental and numerical modeling study. *J. Geophys. Res. Ocean.* **114**, 1–15 (2009).
106. Soto-Navarro, J., Criado-Aldeanueva, F., García-Lafuente, J. & Sánchez-Román, A. Estimation of the Atlantic inflow through the Strait of Gibraltar from climatological and *in situ* data. *J. Geophys. Res. Ocean.* **115** (2010).
107. Sammartino, S. *et al.* Ten years of marine current measurements in Espartel Sill, Strait of Gibraltar. *J. Geophys. Res. Ocean.* **120**, 6309–6328 (2015).

Acknowledgements

Author Contributions

Conceived and designed the study: Y.S.F., J.A., X.A.A.S., A.H.G. Performed the inverse model: M.D.P.H., A.H.G. Performed the organic carbon budget: Y.S.F., X.A.A.S., J.A. Analyzed the data: Y.S.F., X.A.S. Wrote the paper: Y.S.F., X.A.S., E.M., J.A.

Additional Information

Supplementary information accompanies this paper at doi:10.1038/s41598-017-10974-y

Competing Interests: The authors declare that they have no competing interests.

Publisher's note: Springer Nature remains neutral with regard to jurisdictional claims in published maps and institutional affiliations.